J. Astrophys. Astr. (2023) 44:75
https://doi.org/10.1007/s12036-023-09965-5

Estimation of stellar parameters and mass accretion rate of classical T Tauri stars from LAMOST DR6

S. NIDHI*, BLESSON MATHEW, B. SHRIDHARAN, SUMAN BHATTACHARYYA, D. EDWIN and SREEJA S. KARTHA

Department of Physics and Electronics, CHRIST (Deemed to be University), Bangalore 560029, India.
*Corresponding author. E-mail: nidhi.sabu@res.christuniversity.in

MS received 4 November 2022; accepted 12 May 2023

Abstract. Classical T Tauri stars (TTS) are low-mass pre-main sequence stars with an active circumstellar environment. In this work, we present the identification and study of 260 classical TTS using LAMOST Data Release 6, among which 104 stars are newly identified. We distinguish classical TTS from giants and main-sequence dwarfs based on the $\log g$ values, and the presence of Hα emission line and infrared excess that arises from the circumstellar accretion disk. We estimated the mass and age of 210 stars using the Gaia color–magnitude diagram. The age is from 0.1 to 20 Myr, where 90% of the stars have age <10 Myr and the mass ranges between 0.11 and 1.9 $M_{\odot}$. From the measured Hα equivalent widths, we homogeneously estimated the mass accretion rates for 172 stars, with most values ranging from 10^{-7} to 10^{-10} $M_{\odot}$ yr^{-1}. The mass accretion rates are found to follow a power law distribution with the mass of the star, having a relation of the form $\dot{M}_{\rm acc} \propto M_{*}^{1.43\pm0.26}$, in agreement with previous studies.

Keywords. Emission-line star—classical T Tauri stars—accretion.

1. Introduction

Gravitational collapse of cold interstellar clouds gives birth to the dense core in the protostellar phase. The dense core is embedded in the gas and dust associated with the molecular cloud. As it evolves, the embedded gas and dust will disappear, resulting in a circumstellar disk around it (Yoshida *et al.* 2008; Stacy *et al.* 2009). This stage of a star is called pre-main sequence (PMS) phase. PMS stars are young and are found in varying mass and sizes. Generally, they are classified as intermediate-mass and low-mass PMS stars. Young, early-type stars belonging to spectral types B, A, till mid-F-type, with a mass range of 2–10 $M_{\odot}$ are intermediate-mass PMS stars, and those showing emission-lines in their spectrum are Herbig Ae/Be stars (HAeBe; Herbig 1960). The low-mass (<2 $M_{\odot}$) counterparts are T Tauri stars (TTS) which were defined by Joy (1945) as objects associated with nebulosity showing characteristic emission-line spectrum. These stars belong to the spectral type ranging from mid-F-type till late M-type and are found to be systematically brighter than main-sequence stars of the same spectral type (Hillenbrand 1997).

Generally, TTS are classified as classical-T Tauri stars (CTTS) and weak-line T Tauri stars (WTTS). CTTS have strong magnetic fields (Guenther *et al.* 1999; Feigelson *et al.* 2003) through which matter is channeled from the inner circumstellar disk to the stellar surface. The hotspots formed due to the infalling material on the stellar surface results in excess emission in ultraviolet and optical continuum (Koenigl 1991; Gullbring *et al.* 1998; Hartmann *et al.* 2016). Along with these signatures, CTTS show line emission (particularly Hα) and infrared (IR) excess due to the presence of circumstellar disk (Gullbring *et al.* 1998; Muzerolle *et al.* 2003). On the contrary, WTTS present little or no evidence for accretion and IR excess as compared to CTTS (Hartigan *et al.* 1995). Henceforth, WTTS can be assumed to be in a more advanced stage of stellar evolution with no circumstellar accretion disks, indicating the origin of Hα emission line entirely from chromospheric activities (Bertout 1989; Hartmann *et al.* 1994).

This article is part of the Special Issue on "Star formation studies in the context of NIR instruments on 3.6m DOT".

Published online: 28 July 2023

Thus, several studies have proposed IR excess as well as the equivalent width of Hα (EW(Hα)) emission line as criteria to distinguish CTTS from WTTS. In addition, homogeneous spectroscopic studies of these young stellar objects (YSO) opens up the possibility of identifying CTTS and estimating their mass accretion rates (Muzerolle *et al.* 2003; Natta *et al.* 2006; Herczeg & Hillenbrand 2008; Kalari *et al.* 2015; Manara *et al.* 2017).

Generally, the well-studied CTTS from the literature are located around the solar neighborhood or towards the Galactic center (Cieza *et al.* 2007; Barentsen *et al.* 2011; Furlan *et al.* 2011; Rigliaco *et al.* 2012; Herczeg & Hillenbrand 2014; Kalari 2019). In this work, we made use of the data release from the Large Sky Area Multi-Object Fiber Spectroscopic Telescope (LAMOST), to identify young PMS population in the Galactic anti-center direction. Pioneering work in the search of early-type PMS stars using the LAMOST data towards this region were carried out by Hou *et al.* (2016), Anusha *et al.* (2021), Shridharan *et al.* (2021), Zhang *et al.* (2022) and Nidhi *et al.* (2023). These studies have significantly increased the sample of known early-type PMS stars in the galaxy. On the other hand, very few studies on CTTS is carried out in this region, such as that of Lu *et al.* (2018), who found 38 CTTS with X-ray detection and Hα emission line. Also, Zhang *et al.* (2022) identified 20 F-type PMS stars, of which four are TTS. Hence, in this work, we are homogeneously analyzing the CTTS towards the Galactic anti-center region and evaluating the stellar and accretion properties. In Section 2, we discuss the LAMOST survey program and the sample selection method employed to identify the CTTS stars from the LAMOST catalog. Section 3 describes the spatial distribution, evolutionary status and accretion properties of CTTS stars from this study. The results are summarized in Section 4.

2. Data analysis

In this section, we provide a brief overview of the LAMOST telescope and about the observational strategy that provided the data for this study. Also, we explain the step-by-step criteria used to identify CTTS from LAMOST catalog.

2.1 *Defining sample set from LAMOST data release*

The LAMOST is a 4-m quasi-meridian reflecting Schmidt telescope, with a field-of-view of 20 deg^2 (Cui *et al.* 2012; Zhao *et al.* 2012). It is also known as Guo Shoujing Telescope, maintained by Xinglong station of the National Astronomical Observatories, Chinese Academy of Sciences. LAMOST is equipped with 4000 optical fibers in its focal plane and can obtain up to 4000 spectra in one exposure (Zhao *et al.* 2012). The program was initiated in 2012 September and completed the pilot survey and five-years of phase I survey. Phase II of the survey started from 2018 with the 6th data release (DR6[1]), containing 9,911,337 low-resolution spectra (LRS). The LRS has a resolution of $R \sim 1800$ at 5500 Å and wavelength coverage of 3700 Å $\leq \lambda \leq$ 9000 Å. All of the LRS were generally classified into different categories through the pipeline, including 9,231,057 stellar spectra, 177,270 galaxy spectra, 62,168 quasar spectra and 440,842 spectra marked as unknown. We retrieved the spectra of 8,613,842 late-type stars belonging to the spectral type of F5-M9 from the LAMOST DR6 catalog, and is used for our analysis.

2.2 *Procedure for identification of classical TTS*

2.2.1 Finding late-type emission line stars Hα emission line is a prominent feature observed in the emission-line stars (ELS; Kogure & Leung 2007). An automated python routine was used, that employs `find_peaks` function from the `scipy` package to detect the Hα peak within a wavelength window of 6561–6568 Å. Based on the presence of Hα emission line, Edwin *et al.* (in prep) identified 77,586 late-type ELS (LELS) belonging to the spectral type of F5-M9 from LAMOST DR6. We used the 77,586 LELS as our initial sample, in search of CTTS from LAMOST DR6. It was noted that some sources have multiple observations from LAMOST. Hence, we retained the spectrum with signal-to-noise ratio (SNR) in SDSS r-band value >10 ($SNR_r > 10$; Hou *et al.* 2016). This reduced the number of LELS to 56,576. The photometric magnitudes from Gaia DR3 (Gaia Collaboration 2022) mission and its distance estimates from Bailer-Jones *et al.* (2021) are queried for the LELS, resulting in 49,392 stars.

Among 49,392 sources, we noted that 50% of the stars belong to evolved star category (giants/supergiants). These are highly luminous, post-main sequence stars reported to have Hα emission (Rosendhal 1973). The Hα emission in evolved stars primarily originates from wind-driven mass loss (Weymann 1963; Hutchings 1970). Several studies in the literature have categorized evolved stars based on the surface gravity (log *g*), for example, see the studies of Casey *et al.*

[1] https://dr6.lamost.org.

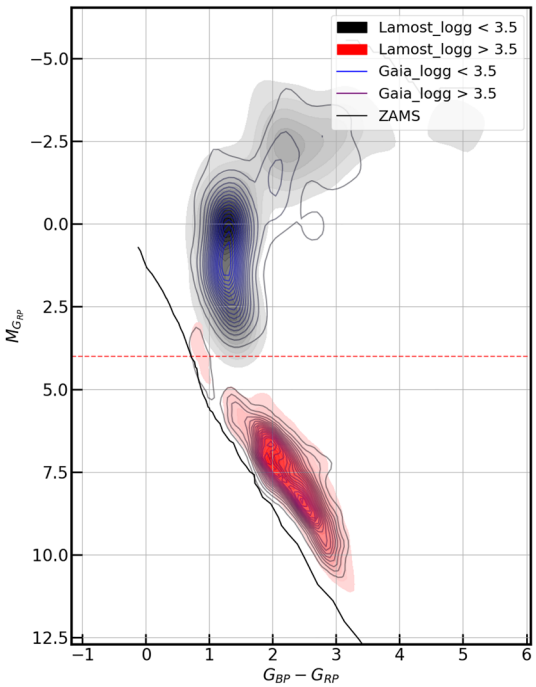

Figure 1. Probability distribution (Gaussian fitted at 20 contour levels) of LELS in the Gaia CMD is represented in the figure. The log g values of LELS from the LAMOST DR6 are shown in black and red shaded colors, respectively. The black shade denotes stars with $\log g < 3.5$, while the red shade denotes stars with $\log g > 3.5$. Also, the log g values of LELS from the Gaia DR3 catalog are displayed as blue and violet line contours, for evolved stars and main sequence stars, respectively. The contours of the blue indicate $\log g < 3.5$ and violet lines indicate $\log g > 3.5$. The red dashed line indicates the $M_{G_{RP}}$ value of 4.0. The black line represents ZAMS from Pecaut & Mamajek (2013).

(2016) ($\log g < 3$), Martell *et al.* (2021) ($3.2 \geq \log g \geq -1.0$) and Frasca *et al.* (2022) ($\log g < 3.5$). In the present work, to separate evolved stars from LELS, we set a threshold of $\log g = 3.5$, as shown in Figure 1. We used the log g values provided by LAMOST DR6, which was estimated using LAMOST stellar parameter pipeline (LASP; Wu *et al.* 2011, Luo *et al.* 2015). Interestingly, log g estimates are available from Gaia DR3 for the sample of stars used in this study. Hence, we were able to assess the reliability of log g values from LAMOST DR6 by comparing it with Gaia DR3 values (Figure 1).

In Figure 1, we have presented the probability distributions (Gaussian fitted at 20 contour levels) of the sample of stars in the Gaia color–magnitude diagram (CMD), in a manner similar to the representation in Bhattacharyya *et al.* (2022). In the CMD plot, we used the Gaia broad-band photometric magnitudes, G_{BP} and G_{RP}, from Gaia DR3 to construct the Gaia CMD. G_{BP} and G_{RP} are corrected for extinction using the 3D dust map of Green *et al.* (2019) and distance estimates from Bailer-Jones *et al.* (2021). From the figure, the distribution makes it evident that the entire LAMOST primary sample can be divided into two parts near $M_{G_{RP}} = 4.0$. The giant branch is surrounded by stars with $\log g < 3.5$, while stars located near to ZAMS are populated with $\log g > 3.5$. Gaia DR3 sample serves as a point of reference for similar distribution, which enables us to confirm the LAMOST data distributions. Since the present work is concerned with CTTS, we removed the stars with $\log g < 3.5$. Henceforth, we consider 24,745 LELS for further analysis.

2.2.2 Selection of CTTS using 2MASS-WISE color–color diagram In CTTS, the IR excess is commonly attributed to the presence of dust in their inner circumstellar disk, which decreases over time as the disk material is dissipated (Cohen & Kuhi 1979; Hartmann *et al.* 2006). Hence, to extract CTTS from LELS, we used the Two Micron All Sky Survey (2MASS; Skrutskie *et al.* 2006) and Wide-field Infrared Survey Explorer (WISE; Cutri *et al.* 2021) IR photometric data to construct a color–color diagram (CCDm). The AllWISE program extends the work of the successful WISE mission by producing a new source catalog and image atlas with enhanced sensitivity and accuracy. However, the AllWISE point source catalog is affected by high numbers of spurious sources, especially in the longer-wavelength bands. Koenig & Leisawitz (2014) recommended a procedure to improve the source reliability in the WISE bands using SNR and reduced chi-squared values (χ^2_ν). The criteria we used in this work is adopted from Koenig & Leisawitz (2014) to suppress false source contamination in WISE $W1$ and $W2$ bands are as follows:

1. WISE band 1: non-null $w1sigmpro$ and $w1rchi2 < (w1snr - 3)/74$.
2. WISE band 2: non-null $w2sigmpro$.

The $w1sigmpro$ and $w2sigmpro$ are the errors in $W1$ and $W2$ magnitudes, respectively. $w1snr$ is the SNR for $W1$ filter and $w1rchi2$ refers to the reduced chi-squared values of the $W2$ profile fit, as provided in the catalog. We also queried J, H and K_s magnitudes from the 2MASS point source catalog (Skrutskie *et al.* 2006). The extinction parameter, A_V, values were retrieved from 3D dust map of Green *et al.* (2019), which were used for further analysis. The reddening corrected 2MASS-WISE CCDm of the LELS is shown in Figure 2. The location of the search box for class II

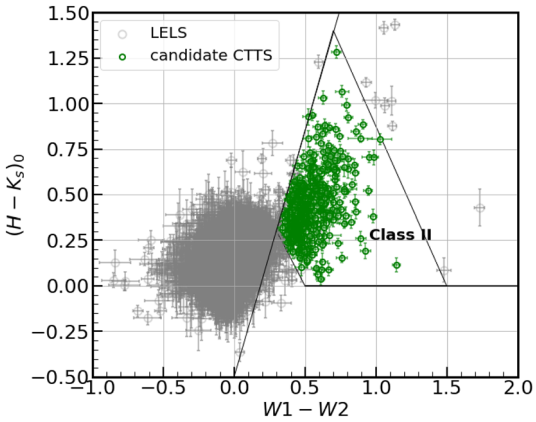

Figure 2. 2MASS-WISE CCD. Gray points represent the LELS point sources. Green points within the polygon represent 374 candidate CTTS belonging to class II category showing IR excess. The YSO selection criteria is adopted from Koenig & Leisawitz (2014).

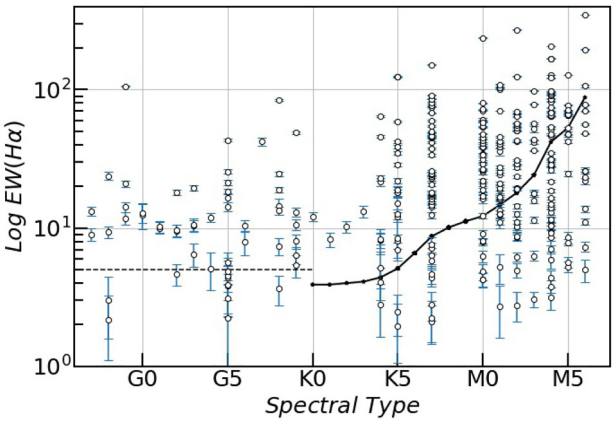

Figure 3. Hα EW for 374 candidate CTTS is plotted against the spectral type. The thick curve represents the Barrado & Martín (2003) to distinguish CTTS from WTTS, for the spectral type from K0 to M7. For stars belonging to F5 to G9 spectral type, a minimum EW(Hα) of 5 Å is represented in a dotted line.

sources in Figure 2 is generated using the YSO search criteria given by Koenig & Leisawitz (2014). Class II is a YSO classification category based on the continuum slope in the IR region of the spectral energy distribution (SED) of the star (Lada 1987; Andre *et al.* 1993). This phase follows that of a protostar, where the star has almost entirely dispersed its envelope, but is still actively accreting from the optically thick accretion disk. We found 374 class II sources showing IR excess and hence, can be considered as candidate CTTS.

2.2.3 Hα *equivalent width as an empirical criterion to identify CTTS* For CTTS, Hα is due to the recombination radiation from the accretion disk. Hence, the emission strength of Hα line is one of the simplest criteria to differentiate the CTTS from WTTS. Martín (1998) proposed the following dependence on the Hα equivalent width (EW(Hα)) of CTTS with respect to the spectral type: 5 Å for spectral types earlier than M0, 10 Å for M0–M2, and 20 Å for later types. White & Basri (2003) also empirically suggested the dependency of EW(Hα) with spectral type. Later, Barrado & Martín (2003) proposed EW(Hα) values as a function of spectral type, derived from the observed saturation limit for the chromospheric activity at $\log(L_{\mathrm{H}\alpha}/L_{\mathrm{bol}}) = -3.3$. Adopting the criterion given by Barrado & Martín (2003) (as shown in Figure 3), we found 213 CTTS stars located above the solid curve. The EW(Hα) is measured using Image Reduction and Analysis Facility (IRAF; Tody 1986) software. It should be noted that only stars belonging to the spectral type ranging from K0 to late M-type can be classified using the above criterion. For rest of the 47 other stars with spectral types from F5 to G9, we put forth a minimum EW(Hα) value of 5 Å based on the criteria given by Martín (1998). Thus, by combining the Hα emission strength and dust emission properties from the accretion disk, we obtained a sample of 260 CTTS, whose spectral properties can be explored further.

3. Results and discussion

The spatial location and stellar properties of 260 CTTS identified from this work are analyzed in this section. We cross-matched our stars with the TTS/YSO catalogs[2] as well as with the SIMBAD database and found identifiers for 156 stars, in which 86 stars are labeled as TTS, six as TTS candidate, 42 as YSO, 12 as YSO candidate and 10 as stars. Though 49 stars from the remaining sample of 104 were mentioned in the study of Škoda *et al.* (2020), they have not classified them into any category of ELS. Hence, through this work, we have identified a new sample of 104 CTTS for which its spatial distribution, stellar and accretion properties are evaluated.

[2]The well-known TTS/YSO catalogs can be retrieved from the studies of Herbst & Shevchenko (1999), Evans *et al.* (2009), Gutermuth *et al.* (2009), Furlan *et al.* (2011), Hsieh & Lai (2013), Herczeg & Hillenbrand (2014), Cottle *et al.* (2018), Briceño *et al.* (2019), Lee *et al.* (2005), Pandey *et al.* (2013), Zuckerman *et al.* (2014) and Zhong *et al.* (2020).

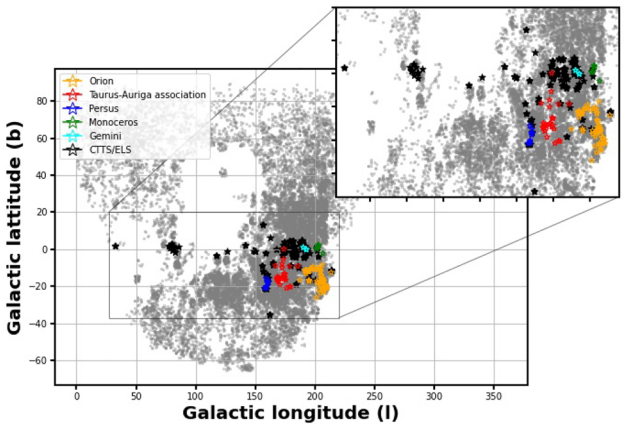

Figure 4. Plot represents the spatial distribution of 260 CTTS stars in Galactic latitude (b) vs. Galactic longitude (l) plane. It can be seen that most of the ELS are found to be within $100° \leq l \leq 220°$ and latitudes $-35° \leq |b| \leq 15°$. The gray points represent the 24,745 LELS. Stars in orange, red, blue, green and cyan colors belong to Orion, Taurus–Auriga association, Perseus, Monoceros and Gemini star-forming regions, respectively. Stars represented in black color are not identified to be part of any star-forming regions.

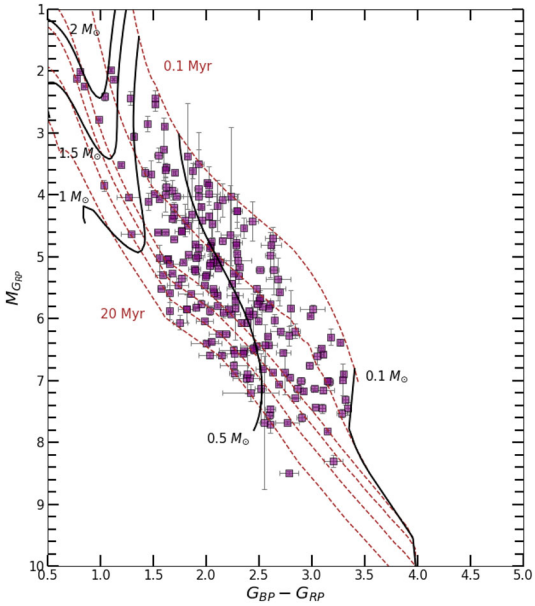

Figure 5. Gaia CMD for CTTS. The isochrones (dashed lines) and tracks (solid lines) are from Bressan *et al.* (2012) at solar metallicity.

3.1 *Spatial distribution of CTTS in Galactic plane*

LAMOST spectroscopic survey of the Galactic anti-center (LSS–GAC) has provided a unique opportunity to explore the distribution of CTTS along the Galactic anti-center direction (Liu *et al.* 2014). The spatial distribution of CTTS is represented in the Galactic coordinates in Figure 4. It is observed that 90% of CTTS are spread over the Galactic longitudes $100° \leq l \leq 220°$ and latitudes $-35° \leq |b| \leq 15°$, implying that the CTTS from this study are spread more towards the Galactic anti-center direction. In Figure 4, we have represented 142 CTTS, based on the star-forming regions with which they are associated. Also, 63 stars are classified as ELS, but they are not reported to be associated with any known star-forming regions. The remaining 55 stars have not been reported in any catalogs and can be considered as new detections. Further investigation on the membership analysis of these stars will be carried out as future work.

3.2 *Stellar properties*

The stellar age (t_*) and mass (M_*) of CTTS are estimated by placing them in the extinction corrected (Section 2.2.1) Gaia CMD and over-plotted with the isochrones and theoretical evolutionary tracks, respectively (Figure 5). We employ Bressan *et al.* (2012) solar metallicity PMS isochrones and tracks to estimate the age and mass for the CTTS.

We obtained the age for 210 CTTS from the Gaia CMD in Figure 5. The age range of CTTS derived from Bressan *et al.* (2012) isochrones is from 0.1 to 20 Myr, where 90% of the stars have age <10 Myr. Similarly, from Figure 5, the mass for 210 CTTS lying above the ZAMS line is estimated from the Gaia CMD, over-plotted with the Bressan *et al.* (2012) evolutionary tracks. The estimated mass range of the CTTS is between 0.11 and 1.9 $M_\odot$. The extinction, distance and estimated age and mass are given in Table 1.

3.3 *Accretion properties*

CTTS have a circumstellar disk from which the matter is accreted onto the stars (Appenzeller & Mundt 1989). In this scenario, the central star has a strong magnetic field producing large starspots. The magnetic field lines truncate the circumstellar disk at a few radii from the star, also known as the truncation radius ($R_{\rm in}$). The matter from the disk gets accreted onto the star through the magnetic field lines, forming accretion columns or funnel flows. The infalling gas moves under free-fall velocities of the order 300 km s^{-1}, causing shocks near the stellar surface. The resulting energy generated from magnetospheric accretion, heats and ionizes the circumstellar gas, thereby causing emission lines (Hartmann *et al.* 2016).

Table 1. Parameters for ten stars are given below. Spectral type from LAMOST, EW(Hα) measured using IRAF, extinction values retrieved from Green *et al.* (2019), distance estimates of these stars obtained from Bailer-Jones *et al.* (2021), estimated age, mass and mass accretion rate for the individual stars from this study are provided. A full version of this table will be made available online.

LAMOST_ID	Spectral type	EW(Hα) (Å)	A_V (mag)	Distance (pc)	Age (Myr)	Mass ($M_\odot$)	$\log(\dot{M}_{\rm acc})$ ($M_\odot$ yr^{-1})
J060413.19+211639.6	F7	-13.2 ± 1	2.3542	$3636.7^{+4803.5}_{-2683.9}$	$0.35^{+0.8}_{-0.1}$	$0.51^{+0.63}_{-0.42}$	$-7.70^{+0.58}_{-0.58}$
J052911.44−060805.4	F7	-8.99 ± 0.94	0.2194	$352.80^{+355.90}_{-349.49}$	$4.5^{+4.8}_{-4.3}$	$1.9^{+1.9}_{-1.9}$	$-6.52^{+1.17}_{-1.08}$
J061509.10+213319.8	F8	-23.8 ± 1.6	1.5334	$1803.0^{+2000.5}_{-1640.6}$	$0.6^{+0.8}_{-0.5}$	$0.48^{+0.55}_{-0.4}$	$-7.76^{+0.55}_{-0.54}$
J051645.56−015122.3	F8	-9.33 ± 0.93	0.4113	$367.86^{+369.71}_{-365.10}$	$4.6^{+4.9}_{-4.3}$	$1.85^{+1.85}_{-1.85}$	$-7.63^{+0.94}_{-1.01}$
J061141.85+203158.9	F9	-11.7 ± 1.2	1.7208	$1813.9^{+2106.2}_{-1572.5}$	$0.1^{+0.3}_{-0.1}$	$0.32^{+0.34}_{-0.29}$	$-8.14^{+0.36}_{-0.53}$
J061544.65+240050.5	F9	-14.2 ± 1.1	1.0695	$1920.3^{+3072.0}_{-1238.3}$	$0.4^{+2}_{-0.1}$	$0.46^{+0.55}_{-0.38}$	$-8.31^{+0.34}_{-0.33}$
J061246.81−061120.9	F9	-20.9 ± 1.1	0.5126	$736.82^{+776.73}_{-695.37}$	$0.45^{+0.5}_{-0.4}$	$0.7^{+0.72}_{-0.56}$	$-7.81^{+0.58}_{-0.58}$
J055532.35+274451.3	F9	-106 ± 0	1.1516	$1217.9^{+1354.0}_{-1098.0}$	$9.3^{+9.8}_{-6.4}$	$0.73^{+0.73}_{-0.72}$	$-8.32^{+0.37}_{-0.38}$
J060747.89+204120.2	G0	-12.4 ± 2.6	1.1403	$1747.6^{+1830.6}_{-1671.6}$	$0.2^{+0.25}_{-0.2}$	$0.7^{+0.61}_{-0.69}$	$-7.17^{+0.54}_{-0.57}$
J055742.67+271929.1	G0	-12.8 ± 1.9	1.0145	$1611.5^{+1698.0}_{-1538.5}$	$0.4^{+0.45}_{-0.35}$	$1.1^{+1.1}_{-1}$	$-7.96^{+0.56}_{-0.56}$

The re-radiated energy can be measured from the emission line luminosity, which is correlated to the accretion luminosity ($L_{\rm acc}$; Alcalá *et al.* 2017). In accreting stars, it has been shown that the major component of Hα emission arises from the accretion funnels and overlaps the emission produced by the accretion shock over the stellar photosphere (Alcalá *et al.* 2017; Frasca *et al.* 2017). We, therefore, determined the Hα line luminosity ($L_{\rm H\alpha}$) from the EW(Hα) to estimate $L_{\rm acc}$. To calculate $L_{\rm H\alpha}$, we first estimate the Hα line flux ($F_{\rm H\alpha}$) using,

$$F_{\rm H\alpha} = W({\rm H\alpha}) \times F_R({\rm H\alpha}), \tag{1}$$

where F_R(Hα) is the continuum flux density at Hα. The F_R(Hα) is calculated using the extinction corrected R band magnitude (R_0, Mathew *et al.* 2018). Further, the $F_{\rm H\alpha}$ is converted to line luminosity using the relationship:

$$L_{\rm H\alpha} = 4\pi d^2 F_{\rm H\alpha}, \tag{2}$$

where d is the distance to the star compiled from Bailer-Jones *et al.* (2021). We used the following relation given in Muzerolle *et al.* (2003) and Barentsen *et al.* (2011) to calculate $L_{\rm acc}$:

$$\log(L_{\rm acc}) = 1.13(\pm 0.07) \times \log(L_{\rm H\alpha}) + 1.93(\pm 0.23). \tag{3}$$

The $\dot{M}_{\rm acc}$ can then be calculated from the free-fall equation:

$$L_{\rm acc} = \frac{G M_* \dot{M}_{\rm acc}}{R_*} \left(1 - \frac{R_*}{R_{\rm in}}\right), \tag{4}$$

where M_* and R_* are the stellar mass and radius, respectively. Based on the previous studies (Gullbring *et al.* 1998; Herczeg & Hillenbrand 2008; Rigliaco *et al.* 2012; Alcalá *et al.* 2014; Manara *et al.* 2016), we adopt $R_{\rm in} = 5R_*$.

The $\dot{M}_{\rm acc}$ is estimated for 172 CTTS, with most values ranging from 10^{-7} to 10^{-10} $M_\odot$ yr^{-1}. The $\dot{M}_{\rm acc}$ of CTTS correlates with the stellar mass, following the power-law relation of $\dot{M}_{\rm acc} \propto M_*^{\alpha}$. In this study, we obtained the power-law of $\dot{M}_{\rm acc} \propto M_*^{1.43\pm0.26}$ as the best fit to the data from this work, which is in agreement with $\dot{M}_{\rm acc} \propto M_*^{1.1\pm0.2}$ obtained by Barentsen *et al.* (2011). In Figure 6, we compared the sample with Barentsen *et al.* (2011) sample, where the stars are found to follow the similar trend with a slope of 0.81 ± 0.17, for the combined sample. Whereas, previous studies have presented higher correlation of accretion rates with stellar mass with $\alpha = 1.8$–2.2 (Muzerolle *et al.* 2003; Natta *et al.* 2006; Herczeg & Hillenbrand 2008; Kalari *et al.* 2015). Fang *et al.* (2009) found $\alpha = 3.1$, which is much steeper than the literature values. The difference in the values is primarily due to the bias in the primary sample. In future work, we aim to conduct a more detailed

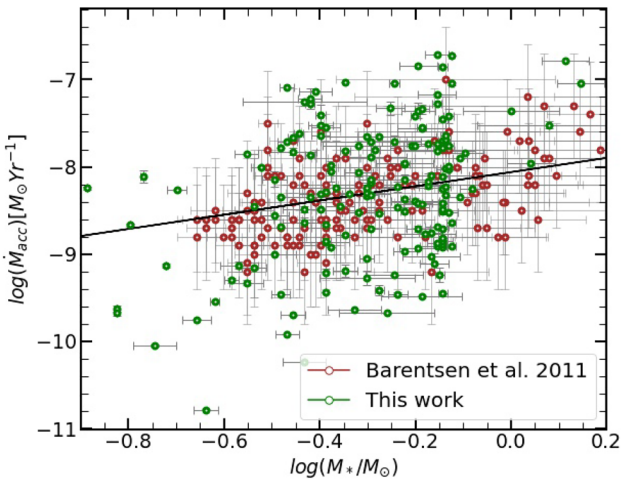

Figure 6. The figure shows the log–log plot between $\dot{M}_{\rm acc}$ and M_* relation of CTTS. Stars from this work are given in green and the sample from Barentsen *et al.* (2011) is given in brown color. The solid black line represents the corresponding best fit to the data with a slope of 0.81 ± 0.17.

investigation into the relationship between the astrometric and spectroscopic parameters in each star-forming region and compare the results.

4. Summary

In this work, we identified a sample of 260 CTTS from LAMOST DR6, most of which are spread towards the Galactic anti-center direction. The initial sample of 77,586 LELS was obtained from Edwin *et al.* (2022; under prep), based on the presence of Hα emission line. To remove the giant stars from our sample, we used the log g threshold of 3.5. Then, to identify young stars with IR excess, we made use of 2MASS-WISE CCDm after the prescribed quality cuts. Finally, we identified 260 bonafide CTTS from the initial sample, in which 104 stars are newly identified. It is seen that our sample of CTTS are spatially found to be within $100^\circ \leq l \leq 220^\circ$ and latitudes $-35^\circ \leq |b| \leq 15^\circ$, which is also color-coded with respect to the star-forming region associated with it. We used Gaia DR3 photometric values to estimate the stellar parameters, such as mass and age of identified CTTS. The age range of CTTS is from 0.1 to 20 Myr, with 90% of the stars having age <10 Myr. Also, the estimated mass range of the CTTS is between 0.11 and 1.9 $M_\odot$. Using the age and mass estimates, we derived the $\dot{M}_{\rm acc}$ for 172 CTTS, which ranges from 10^{-7} to 10^{-10} $M_\odot$ yr^{-1}. The values are tabulated in Table 1. We found a clear trend of mass accretion rates increasing as a function of stellar mass. Irrespective of the location of the stars, either in Galactic center or Galactic anti-center directions, the power-law relationship obtained for our stars, $\dot{M}_{\rm acc} \propto M_*^{1.43\pm0.26}$ is found to be in agreement with the literature.

Acknowledgements

We thank Cysil Baby Tom for his valuable suggestions in this work. We are grateful to the Centre for Research, CHRIST (Deemed to be University), Bangalore, for the research grant extended to carry out the present project (MRPDSC-1932). Also, we would like to thank the Science & Engineering Research Board (SERB), a statutory body of Department of Science & Technology (DST), Government of India, for funding our research under grant number CRG/2019/005380. This work has made use of data products from the Guo Shoujing Telescope (the Large Sky Area Multi-Object Fibre Spectroscopic Telescope, LAMOST) and data from the European Space Agency (ESA) mission Gaia (https://www.cosmos.esa.int/gaia), processed by the Gaia Data Processing and Analysis Consortium (DPAC, https://www.cosmos.esa.int/web/gaia/dpac/consortium). Funding for the DPAC has been provided by national institutions, in particular, the institutions participating in the Gaia Multilateral Agreement. We thank the SIMBAD database and the online VizieR library service for helping us in literature survey and in obtaining relevant data.

References

Alcalá J. M., Natta A., Manara C. F. *et al.* 2014, Astronomy & Astrophysics, 561, A2
Alcalá J. M., Manara C. F., Natta A. *et al.* 2017, Astronomy & Astrophysics, 600, A20
Andre P., Ward-Thompson D., Barsony M. 1993, Astrophysical Journal, 406, 122
Anusha R., Mathew B., Shridharan B. *et al.* 2021, Monthly Notices of the Royal Astronomical Society, 501, 5927
Appenzeller I., Mundt R. 1989, The Astronomy and Astrophysics Review, 1, 291
Bailer-Jones C. A. L., Rybizki J., Fouesneau M., Demleitner M., Andrae R. 2021, The Astronomical Journal, 161, 147
Barentsen G., Vink J. S., Drew J. E. *et al.* 2011, Monthly Notices of the Royal Astronomical Society, 415, 103
Barrado y Navascués D., Martín E. L. 2003, The Astronomical Journal, 126, 2997
Bertout C. 1989, Annual Rev. Astron. Astrophys, 27, 351
Bhattacharyya S., Mathew B., Ezhikode S. H. *et al.* 2022, The Astrophysical Journal Letters, 933, L34
Bressan A., Marigo P., Girardi L. *et al.* 2012, Monthly Notices of the Royal Astronomical Society, 427, 127

Briceño C., Calvet N., Hernández J. *et al*. 2019, The Astrophysical Journal, 157, 85
Casey A. R., Ruchti G., Masseron T. *et al*. 2016, Monthly Notices of the Royal Astronomical Society, 461, 3336
Cieza L., Padgett D. L., Stapelfeldt K. R. *et al*. 2007, The Astrophysical Journal, 667, 308
Cohen M., Kuhi L. V. 1979, The Astrophysical Journal Supplement, 41, 743
Cottle J. N., Covey K. R., Suárez G. *et al*. 2018, The Astrophysical Journal Supplement, 236, 27
Cui X.-Q., Zhao Y.-H., Chu Y.-Q. *et al*. 2012, Research in Astronomy and Astrophysics, 12, 1197
Cutri R. M., Wright E. L., Conrow T. *et al.* 2021, VizieR Online Data Catalog, II/328
Evans Neal J., I., Dunham M. M., Jørgensen J. K. *et al.* 2009, The Astrophysical Journal Supplement, 181, 321
Fang M., van Boekel R., Wang W. *et al*. 2009, Astronomy & Astrophysics, 504, 461
Feigelson E. D., Gaffney J. A. III., Garmire G., Hillenbrand L. A., Townsley L. 2003, Astrophysical Journal, 584, 911
Frasca A., Biazzo K., Alcalá J. M. *et al*. 2017, Astronomy & Astrophysics, 602, A33
Frasca A., Molenda-Żakowicz J., Alonso-Santiago J. *et al*. 2022, Astronomy & Astrophysics, 664, A78
Furlan E., Luhman K. L., Espaillat C. *et al*. 2011, The Astrophysical Journal Supplement, 195, 3
Gaia Collaboration, 2022, VizieR Online Data Catalog, I/355
Green G. M., Schlafly E., Zucker C., Speagle J. S., Finkbeiner D. 2019, The Astrophysical Journal, 887, 93
Guenther E. W., Lehmann H., Emerson J. P., Staude J. 1999, Astronomy & Astrophysics, 341, 768
Gullbring E., Hartmann L., Briceño C., Calvet N. 1998, The Astrophysical Journal, 492, 323
Gutermuth R. A., Megeath S. T., Myers P. C. *et al*. 2009, The Astrophysical Journal Supplement, 184, 18
Hartigan P., Edwards S., Ghandour L. 1995, The Astrophysical Journal, 452, 736
Hartmann L., D'Alessio P., Calvet N., Muzerolle J. 2006, The Astrophysical Journal, 648, 484
Hartmann L., Herczeg G., Calvet N. 2016, Annual Rev. Astron. Astrophys., 54, 135
Hartmann L., Hewett R., Calvet N. 1994, The Astrophysical Journal, 426, 669
Herbig G. H. 1960, The Astrophysical Journal Supplement, 4, 337
Herbst W., Shevchenko V. S. 1999, The Astrophysical Journal, 118, 1043
Herczeg G. J., Hillenbrand L. A. 2008, The Astrophysical Journal, 681, 594
Herczeg G. J., Hillenbrand L. A. 2014, The Astrophysical Journal, 786, 97
Hillenbrand L. A. 1997, The Astrophysical Journal, 113, 1733
Hou W., Luo A. L., Hu J.-Y. *et al*. 2016, Research in Astronomy and Astrophysics, 16, 138
Hsieh T.-H., Lai S.-P. 2013, The Astrophysical Journal Supplement, 205, 5
Hutchings J. B. 1970, Monthly Notices of the Royal Astronomical Society, 147, 161
Kalari V. M. 2019, Monthly Notices of the Royal Astronomical Society, 484, 5102
Kalari V. M., Vink J. S., Drew J. E. *et al*. 2015, Monthly Notices of the Royal Astronomical Society, 453, 1026
Koenig X. P., Leisawitz D. T. 2014, The Astrophysical Journal, 791, 131
Koenigl A. 1991, Astrophysical Journal Letters, 370, L39
Kogure T., Leung K.-C. 2007, The Astrophysics of Emi-ssion-Line Stars 342, https://doi.org/10.1007/978-0-387-68995-1
Lada C. J. 1987, in Star Forming Regions, eds Peimbert M., Jugaku J., Vol. 115, p. 1
Lee H.-T., Chen W. P., Zhang Z.-W., Hu J.-Y. 2005, The Astrophysical Journal, 624, 808
Liu X. W., Yuan H. B., Huo Z. Y. *et al.* 2014, in Setting the scene for Gaia and LAMOST, eds Feltzing S., Zhao G., Walton N. A., Whitelock P., Vol. 298, p. 310
Lu H.-P., Zhang L.-Y., Han X. L., Shi J. 2018, Astrophysics and Space Science, 363, 104
Luo A. L., Zhao Y.-H., Zhao G. *et al*. 2015, Research in Astronomy and Astrophysics, 15, 1095
Manara C. F., Rosotti G., Testi L. *et al*. 2016, Astronomy & Astrophysics, 591, L3
Manara C. F., Testi L., Herczeg G. J. *et al*. 2017, Astronomy & Astrophysics, 604, A127
Martell S. L., Simpson J. D., Balasubramaniam A. G. *et al*. 2021, Monthly Notices of the Royal Astronomical Society, 505, 534
Martín E. L. 1998, The Astronomical Journal, 115, 351
Mathew B., Manoj P., Narang M. *et al*. 2018, The Astrophysical Journal, 857, 30
Muzerolle J., Hillenbrand L., Calvet N., Briceño C., Hartmann L. 2003, The Astrophysical Journal, 592, 266
Natta A., Testi L., Randich S. 2006, Astronomy & Astrophysics, 452, 245
Nidhi S., Mathew B., Shridharan B. *et al.* 2023, arXiv e-prints, arXiv:2307.02917
Pandey A. K., Eswaraiah C., Sharma S. *et al*. 2013, The Astrophysical Journal, 764, 172
Pecaut M. J., Mamajek E. E. 2013, The Astrophysical Journal Supplement, 208, 9
Rigliaco E., Natta A., Testi L. *et al*. 2012, Astronomy & Astrophysics, 548, A56
Rosendhal J. D. 1973, The Astrophysical Journal, 186, 909
Shridharan B., Mathew B., Nidhi S. *et al*. 2021, Research in Astronomy and Astrophysics, 21, 288
Škoda P., Podsztavek O., Tvrdík P. 2020, Astronomy & Astrophysics, 643, A122
Skrutskie M. F., Cutri R. M., Stiening R. *et al.* 2006, 131, 1163
Stacy A., Greif T. H., Bromm V. 2009, in Astronomical Society of the Pacific Conference Series, Vol. 419, Galaxy

Evolution: Emerging Insights and Future Challenges, eds Jogee S., Marinova I., Hao L., Blanc G. A., p. 339
Tody D. 1986, in Society of Photo-Optical Instrumentation Engineers (SPIE) Conference Series, Instrumentation in Astronomy VI, ed Crawford D. L., Vol. 627, p. 733
Weymann R. 1963, Annual Rev. Astron. Astrophys., 1, 97
White R. J., Basri G. 2003, The Astrophysical Journal, 582, 1109
Wu Y., Luo A. L., Li H.-N. *et al*. 2011, Research in Astronomy and Astrophysics, 11, 924
Yoshida N., Omukai K., Hernquist L. 2008, Science, 321, 669
Zhang Y.-J., Luo A. L., Jiang B. *et al*. 2022, The Astrophysical Journal, 936, 151
Zhao G., Zhao Y., Chu Y., Jing Y., Deng L. 2012, arXiv e-prints, arXiv:1206.3569
Zhong J., Chen L., Wu D. *et al*. 2020, Astronomy & Astrophysics, 640, A127
Zuckerman B., Vican L., Rodriguez D. R. 2014, The Astrophysical Journal, 788, 102